Chapter 6 Morphology/ Substrate Dependent MoS_2 Based SERS Biosensors

6.1 Introduction

The detection and quantification of biomolecules is an essential perspective in medical and biochemical applications, and has become a research hotspot owing to advancement of recent technologies in clinical diagnosis for quick and precise ultra-trace detection. Bilirubin is a type of hydrophobic toxin, that requires urgent early diagnosis of hemolytic disorders in both adults and infants. More specifically, high free bilirubin (>50 μM, called hyperbilirubinemia) leads to metabolic disorder causing jaundice, liver problem, biliary tract dysfunction, brain damage and even death in cases of neonates. On the other hand, low bilirubin concentration in serum may evoke complications like coronary heart diseases and iron deficiency [73, 198, 199]. Thus, identifying the accurate bilirubin concentration is essential for the early diagnosis of bilirubin-induced diseases. Another essential biomolecule for the proper functioning of the metabolism is vitamin B. In this group, cobalamin (vitamin B_{12}) is a cobalt-containing water-soluble vitamin. Among the major forms of cobalamin, cyanocobalamin is the most stable active one, which is crucial for DNA synthesis, formation of red blood cells and the preservation of neurological operations. Its deficiency is associated with dementia and Alzheimer diseases [74, 200]. So, its rapid and efficient detection is crucial to identify its concentration in human blood samples. Various analytical methods such as high-performance liquid chromatography (HPLC), colorimetry, mass spectrometry, fluorimetry, amperometry, etc. have been used to quantify the concentration of these biomolecules, but have restraints in terms of sample treatment, instrumentation requirement, professional operators, cost and time [74, 201]. Among spectroscopy techniques, Raman spectroscopy is a fast, non-destructive and versatile analytical tool for molecule sensing. However, the ultra-trace molecule detection is

difficult with this technique, owing to low scattering probability, until the discovery of surface-enhanced Raman spectroscopy (SERS). **Figure 6.1 (a)** provides a schematic illustration of the SERS process. The high sensitivity of SERS relies on two widely accepted mechanisms: Electromagnetic (EM) and Chemical (CM) enhancements [202-205].

(a) Electromagnetic (EM) Mechanism: The EM mechanism is typically associated with metallic substrates and arises because of localized surface plasmon resonance (**Figure 6.1 (b)**). Surface plasmons refer to collective oscillations of electrons within the electron gas of a metal and are confined to the near surface region. The size and shape of these metallic nanostructures determine the resonance frequency at which the surface plasmons will oscillate in response to the incoming light. When the frequency of the incident light matches the resonant frequency of these surface plasmons, it leads to a phenomenon known as localized surface plasmon resonance (LSPR). During LSPR, the collective oscillations of electrons on the surface of these nanostructures become highly amplified. This amplification results in a significant enhancement of the electromagnetic field near the metal surface and amplifies the Raman signal of nearby molecules.

(b) Chemical (CM) Enhancements: The CM mechanism is related to the semiconducting substrates and emerges as a result of chemical interaction between the SERS substrate and analyte molecules (**Figure 6.1 (b)**). This phenomenon is also referred as the charge transfer (CT) mechanism, as it involves the photoinduced transfer of an electron from the valence/conduction band (VB/CB) of the SERS substrate to the highest occupied/lowest unoccupied molecular orbitals (HOMO/LUMO) of the analyte molecule or vice versa, depending upon their relative location and on the energy of the incident photon.

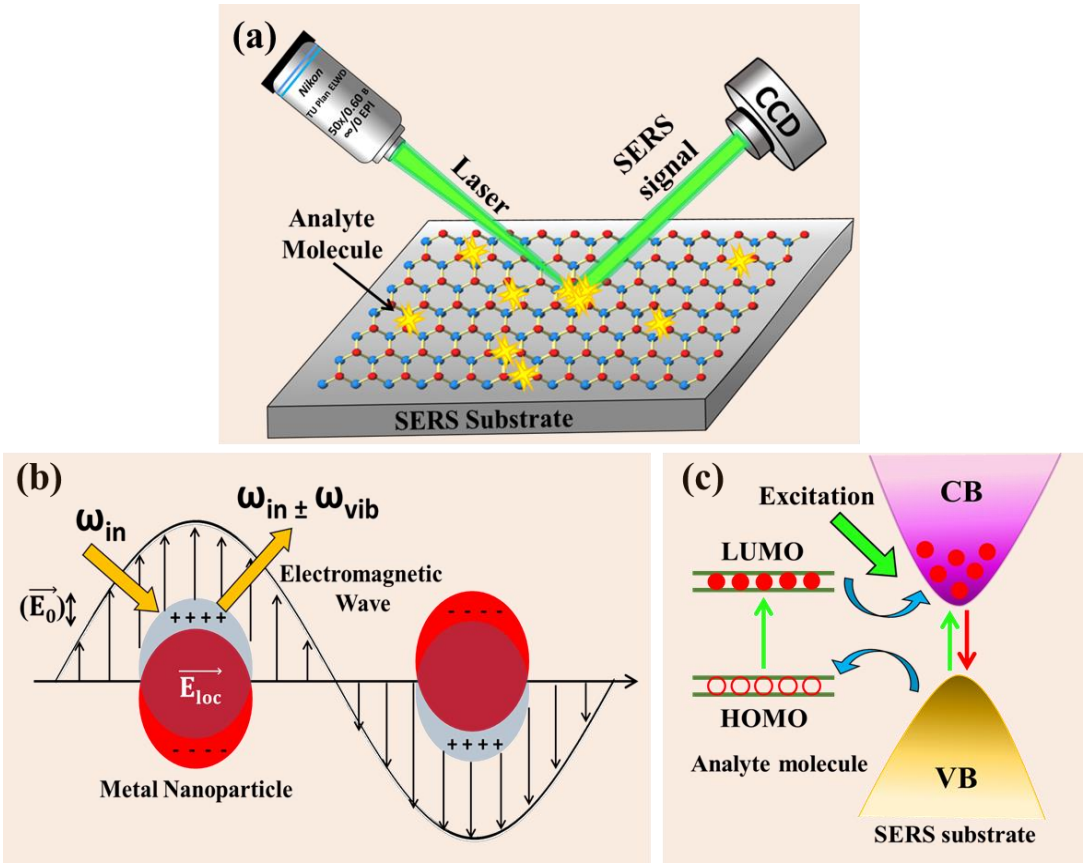

Figure 6.1 *Schematic illustrating the (a) SERS process, (b) Electromagnetic enhancement and (c) Chemical enhancement.*

Semiconducting substrates being low cost, stable, abundant and their easy integration with electronic devices have made them to be widely investigated as SERS substrate [206, 207]. Among semiconductors, two-dimensional (2D) layered transition metal dichalcogenide (TMD) nanomaterials are new possibilities for SERS candidates owing to their unique features like quantum confinement, tunable bandgap, high carrier mobility, excellent biocompatibility, large surface area with accessible edges, high chemical stability and distinctive charge transfer capability [208, 209]. The quantum confinement in layered TMDs may result in significant bandgap change, leading to enhanced photoluminescence (PL) and SERS signal. Fermi's golden law states that the electron transition probability is linearly associated with the density of states close to the fermi level in charge transfer (CT) process [210]. The TMDs have numerous energy states close to the fermi level and show active interaction with analytes, proving them appropriate candidate for SERS applications. Among them, MoS_2 emerges as a

recent platform for SERS due to its visible bandgap, remarkable adsorption capacity and fluorescence quenching feature [211, 212]. The bandgap of MoS_2 can be modulated from 1.2 to 1.9 eV by varying layer number [213], showing its flexibility and light absorption capability. The Raman enhancement for MoS_2 as a SERS substrate comprises charge transfer and dipole-dipole coupling, owing to its semiconducting feature and chemical bonds of polar covalent bond (Mo-S) [214]. As far as synthesis is concerned, mechanical exfoliation, hydrothermal/solvothermal method, chemical vapor deposition (CVD), magnetron sputtering, etc. can be utilized for the synthesis of MoS_2 nanostructures [93, 215-217]. Among all, CVD technique is a highly flexible, facile and efficient approach for the large area growth with varying morphologies, offering great potential for SERS application. Different MoS_2 nanostructures provide different surface roughness and active sites, which can enhance the light trapping efficiency and better adsorption of analytes to improve SERS detection. Also, the electrical properties of MoS_2 grown on different substrates can be modulated by the underlying substrate, that leads to different CT mechanism and hence different SERS activity [218, 219]. For enhancing the SERS signal, many strategies have been proposed that enhance the photo-induced charge transfer (PICT) efficiency between the SERS substrate and analyte biomolecules. One of the promising strategy is low temperature study that decreases the non-radiative recombination by declining the thermal vibration of the lattice and promoting more photo-induced electrons to take part in PICT process.

6.2 Sample Preparation for SERS Measurement

Synthesis of SERS substrates (H-MoS_2/FTO, V-MoS_2/Si, V-MoS_2/SiO_2-Si and H-MoS_2/SiO_2-Si) have already been discussed in **section 2.1** of **chapter 2**. A stock solution (10^{-3} M) of bilirubin and vitamin B_{12} (cyanocobalamin) were prepared in Milli-Q water at room temperature with ultrasonic treatment for 4-5 hours. Solutions of different concentrations ranging from 10^{-4} to 10^{-12} M and 10^{-4} to 10^{-9} M of bilirubin and vitamin B_{12} were prepared

from the stock solution of both the biomolecules using serial dilution method, as shown in **Figure 6.2 (a, b)**, respectively. At higher concentration, the color of biomolecules is visible, that gradually becomes transparent at lower concentration and hence their detection is difficult. The as-synthesized MoS_2 nanostructures on different substrates were cut into small pieces and 2 µL of each biomolecule with different concentrations were dropped successively on all the substrates and kept for 3-4 hrs in vacuum for drying.

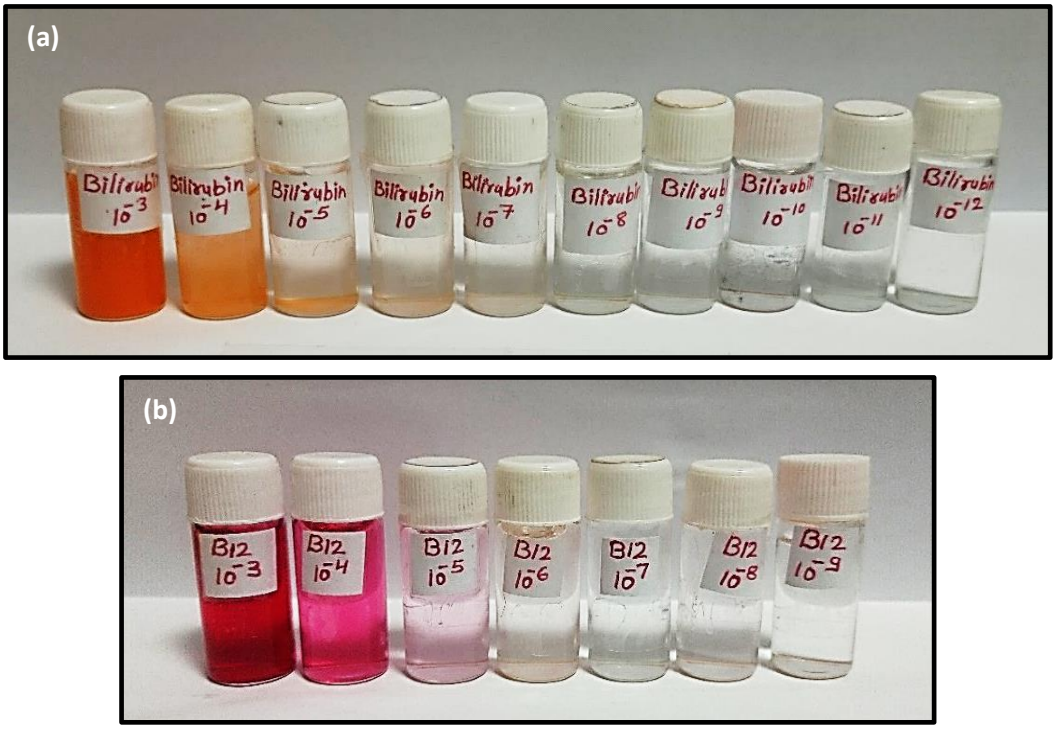

Figure 6.2 *Photographs showing the different concentrations of (a) bilirubin biomolecule from 10^{-3} to 10^{-12} M and (b) vitamin B_{12} (cyanocobalamin) from 10^{-3} to 10^{-9} M.*

6.3 Results and Discussion

6.3.1 Characterization of Dye Molecules

The Raman spectra of bulk bilirubin and vitamin B_{12} biomolecules were obtained with 633 and 532 nm excitation laser, as shown in **Figure 6.3 (a, b)**, respectively. The assignments of the dominant Raman peaks of bilirubin and vitamin B_{12} are listed in **Table 6.1** and **Table 6.2**, respectively.

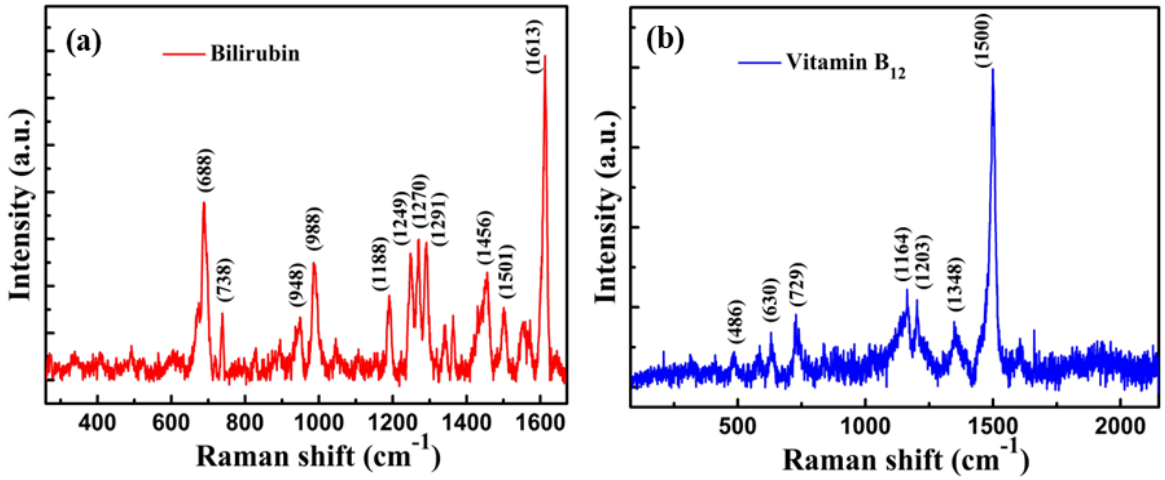

Figure 6.3 *Raman spectra of (a) bulk bilirubin collected using 633 nm excitation laser and (b) bulk vitamin B_{12} biomolecules collected using 532 nm excitation laser.*

Table 6.1 Assignments of bands of bilirubin biomolecules using 633 nm excitation [198, 220].

Raman Shift (cm^{-1})	**Assignment**	**Raman Shift (cm^{-1})**	**Assignment**
688	Twisting of C=O bond in COOH group	1291	CH bending
738	Out-of-plane ring deformation	1342	CCH bending in CH_3
948	Out-of-plane CH vibration	1363	CH_2 scissoring
988	CH_3 asymmetric deformation	1456	C-C and C-N mixed stretching
1188	CH_3 out-of-plane bending and C-C stretching	1501	C=C stretching in ring and C-C stretching between ring and $CH=CH_2$
1249	CCH bending and CCC bending	1571	Asymmetric C-N stretching in ring
1270	Stretching and bending	1613	C=C stretching in five-membered ring

Table 6.2 Assignments of bands of vitamin B_{12} biomolecules using 532 nm excitation [221, 222].

Raman Shift (cm^{-1})	Assignment
486	Corrin ring vibration modes
630	Co–CN stretching mode
729	5,6-Dimethylbenzimidazole vibrational modes
1164	Stretching of C–C and C–N mode in addition to the CH bending, CH_2 twisting and CH_3 rocking modes
1203	Stretching of C–C bond in addition to the CH bending, CH_2 twisting and CH_3 rocking modes
1348	Vibrational stretching of N_2–C_6 and N_3–C_{14} bonds, with respect to the Co–C_{10} axis
1500	Stretching of C=C and C=N bonds of the corrin ring with some contributions from CH, CH_2 and CH_3 bending modes

6.3.2 Characterization of SERS Substrates

The SEM images of as-synthesized MoS_2 nanostructures on different substrates illustrate the large area coverage and distinct morphologies of the grown film. The SEM image of H-MoS_2/FTO is shown in **Figure 6.4 (a)**, indicating the growth of large area continuous thin film of MoS_2 over FTO substrate. The SEM image of H-MoS_2/FTO at higher magnification (**Figure 6.4 (b)**) reveals the surface roughness of MoS_2 film, which is favourable for biomolecule adsorption and light harvesting for high SERS activity. The SEM images of V-MoS_2/Si (**Figure 6.4 (c, d)**) shows the large-scale formation of interconnected vertically oriented 3D network of edge-enriched MoS_2 nanoflakes. The morphology shows larger nucleation sites (more homogeneous network), high growth rate (bigger nanoflake size) and nearly vertical orientation that may provide more accessible surface area for better biomolecule adsorption on V-MoS_2/Si SERS substrate along with better light absorption by multiple reflection among nanoflakes. These densely stacked vertical nanoflakes are believed to contribute for greater SERS enhancement. The vertical and horizontal growth of MoS_2

nanostructures on SiO_2-Si substrate are shown in **Figure 6.4 (e, g)**, respectively. Compared to V-MoS_2/Si, V-MoS_2/SiO_2-Si nanoflakes have smaller lateral dimensions and heights as shown in **Figure 6.4 (f)**. The higher magnification SEM image of H-MoS_2/SiO_2-Si (**Figure 6.4 (h)**) shows that the randomly oriented MoS_2 triangular domains are the nucleation sites for the horizontal growth. The size of these domain increases with growth time and coalesce to form a film. The portion of continuous film formation seems to be high, based on coverage domain to the overall grown region. Differently grown MoS_2 nanostructures were also characterized using Raman spectroscopy with 532 nm excitation, as displayed in **Figure 2.13 (b)** of **chapter 2**. The observed frequency differences validate the growth of few-layer MoS_2 nanostructures on different substrates. The Raman spectra of these MoS_2 nanostructures grown over different substrates using 633 nm laser excitation are shown in **Figure 2.13 (d)** of **chapter 2**. The semiconducting behavior of synthesized MoS_2 nanostructures on different substrates were examined via PL study (**Figure 2.15 (b)** of **chapter 2**). The existence of direct excitons assists the charge transfer between the SERS substrate and the biomolecules showing efficient SERS detection. When the analyte molecules are adsorbed on these MoS_2 nanostructures, its semiconducting behavior and light trapping capability can facilitate the SERS detection of the biomolecules at lower concentrations.

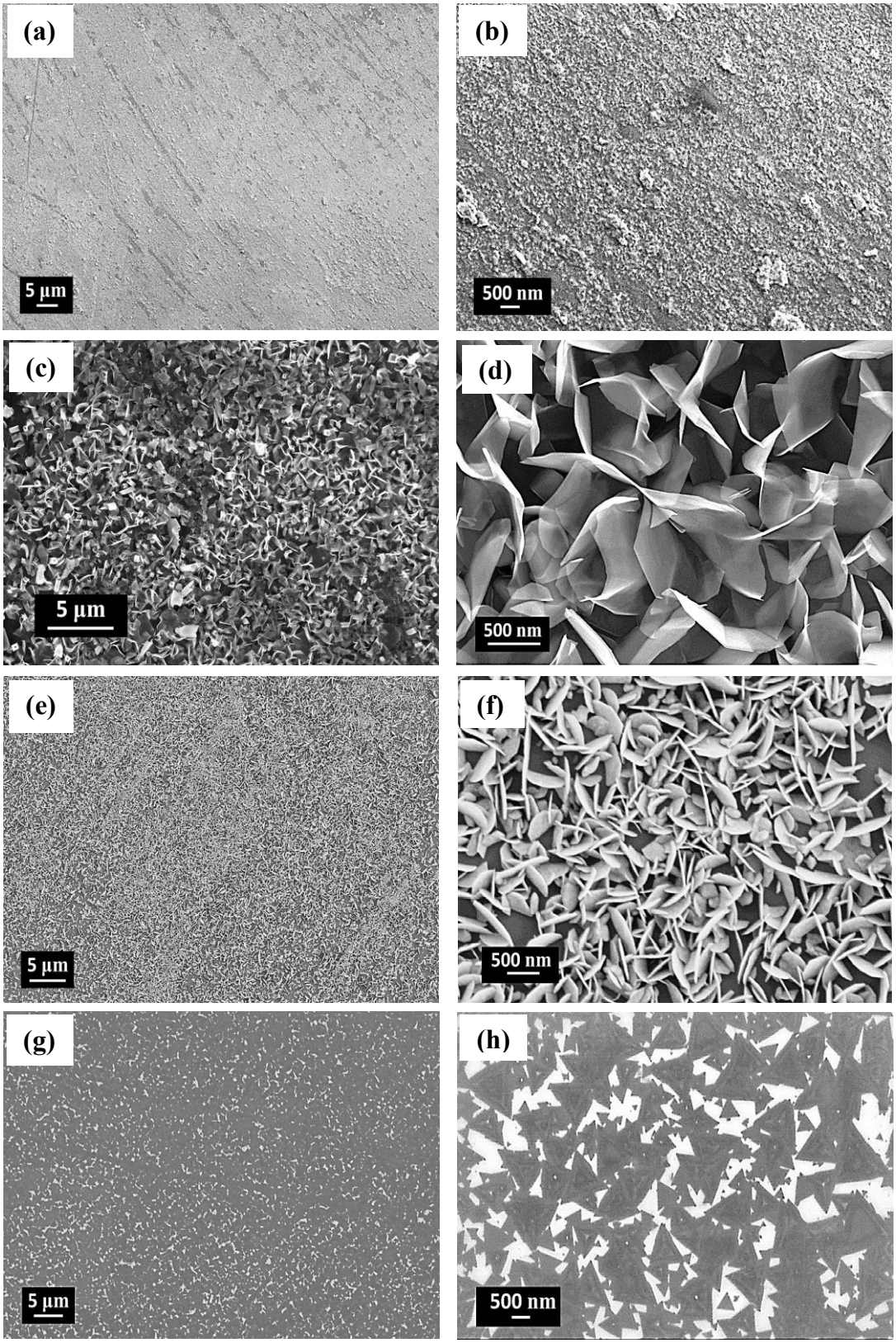

Figure 6.4 *SEM images of (a,b) H-MoS_2/FTO, (c,d) V-MoS_2/Si, (e,f) V-MoS_2/SiO_2-Si and (g,h) H-MoS_2/SiO_2-Si.*

6.3.3 SERS Application for the Detection of Bilirubin using Different Prepared MoS_2 Nanostructures

The SERS spectra of different concentrations of bilirubin biomolecule are obtained over H-MoS_2/FTO, V-MoS_2/Si, V-MoS_2/SiO_2-Si and H-MoS_2/SiO_2-Si SERS substrates. The peak positions of bilirubin biomolecule are slightly shifted compared to Raman spectrum of bulk bilirubin powder, when adsorbed on different SERS substrates, indicating the charge transfer between the bilirubin biomolecule and SERS substrate [223]. We observe that the SERS intensity decreases as the bilirubin concentration decreases, and thus no SERS peak of bilirubin is observed at 10^{-12} M for H-MoS_2/FTO and V-MoS_2/Si, at 10^{-10} M for V-MoS_2/SiO_2-Si and at 10^{-9} M for H-MoS_2/SiO_2-Si SERS substrate. The significant intensities of bilirubin SERS peak at 10^{-11} M concentration in case of H-MoS_2/FTO (**Figure 6.5 (a, b)** and V-MoS_2/Si (**Figure 6.5 (c, d)**, illustrates the ultrasensitive detection of bilirubin on both the SERS substrate, compared to V-MoS_2/SiO_2-Si (10^{-9} M, **Figure 6.5 (e, f))** and H-MoS_2/SiO_2-Si (10^{-8} M, **Figure 6.5 (g)**). The intense peak at ~1613 cm^{-1} (C=C stretching in five-membered ring) is chosen here for the detection of bilirubin. Moreover, the quantitative well-defined linear relationships between the SERS intensity of bilirubin at ~1613 cm^{-1} with different concentrations on different SERS substrates are depicted in **Figure 6.5 (h)**. Meanwhile, the SERS mapping of different concentrations of bilirubin on different SERS substrates (10^{-9} M for H-MoS_2/FTO and V-MoS_2/Si, 10^{-7} M for V-MoS_2/SiO_2-Si and 10^{-6} M for H-MoS_2/SiO_2-Si) are shown in **Figure 6.6** to **Figure 6.9**, respectively. In bilirubin mapping, the Raman peak of MoS_2 at ~457 cm^{-1} and the characteristic SERS peak of bilirubin (~1613 cm^{-1}) are shown by red and green color, respectively. The SERS mapping clearly indicates that our synthesized SERS substrate provides high uniformity for biomolecule adsorption.

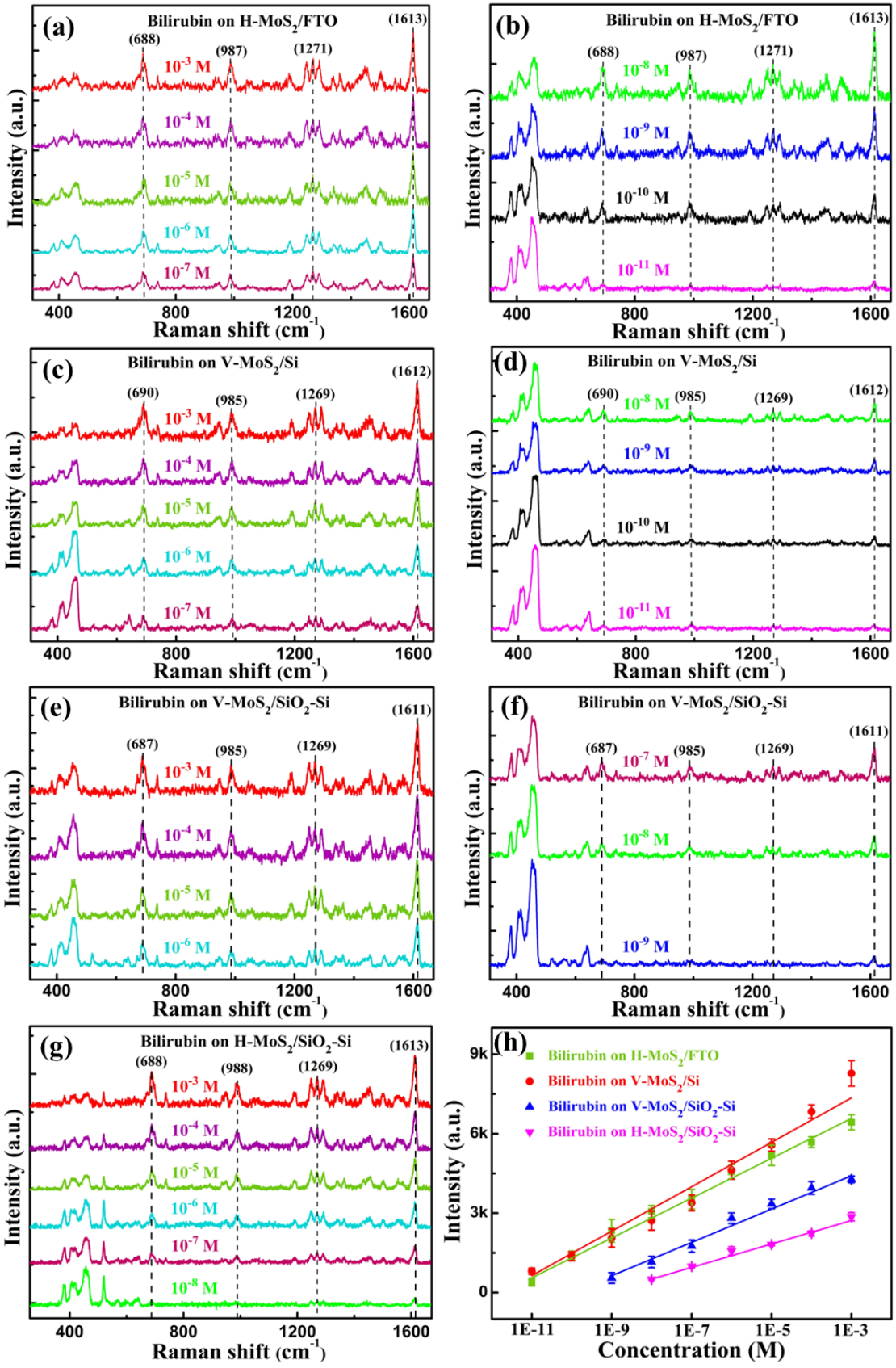

Figure 6.5 *SERS spectra of bilirubin biomolecule at different concentrations on (a,b) H-MoS2/FTO, (c,d) V-MoS2/Si, (e,f) V-MoS2/SiO2-Si and (g) H-MoS2/SiO2-Si SERS substrates. (h) Raman intensity of characteristic peak versus bilirubin concentrations on these substrates.*

(i) SERS Mapping of Bilirubin on H-MoS_2/FTO SERS Substrate

The SERS spectrum and mapping of 10^{-9} M bilirubin adsorbed over H-MoS_2/FTO SERS substrate are shown in **Figure 6.6 (a)** and inset, respectively. The SERS peak of MoS_2 at ~457 cm^{-1} and of bilirubin at ~1613 cm^{-1} are shown by red and green color in **Figure 6.6 (b, c)**, respectively. This clearly indicates the uniform distribution of bilirubin biomolecule adsorbed over H-MoS_2/FTO SERS substrate.

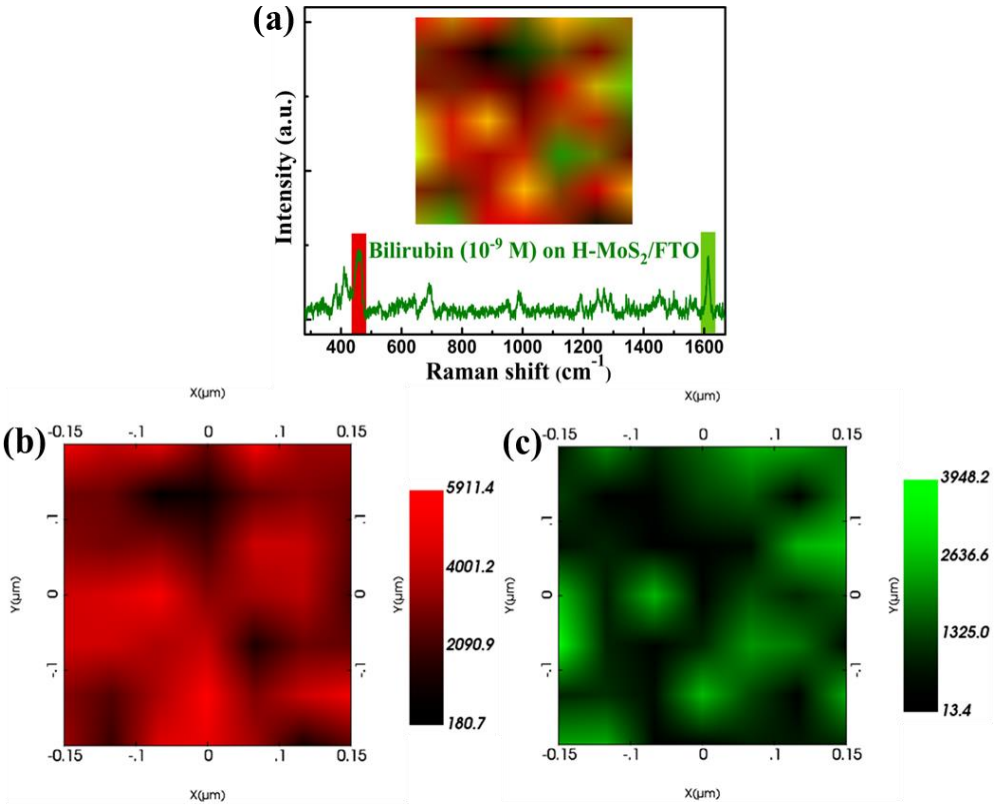

Figure 6.6 *(a) SERS spectrum and mapping of (b) MoS_2 (~457 cm^{-1}, shown by red color) and (c) bilirubin (~1613 cm^{-1}, shown by green color) on H-MoS_2/FTO substrate. Inset of (a) shows the SERS mapping of bilirubin adsorbed over H-MoS_2/FTO.*

(ii) SERS Mapping of Bilirubin on V-MoS_2/Si SERS Substrate

Similarly, the SERS spectrum and mapping of 10^{-9} M bilirubin adsorbed over V-MoS_2/Si SERS substrate are shown in **Figure 6.7 (a)** and inset, respectively, indicating uniform distribution of bilirubin biomolecule adsorbed over V-MoS_2/Si SERS substrate. The SERS peak of MoS_2 at

~457 cm^{-1} and of bilirubin at ~1612 cm^{-1} are shown by red and green color in **Figure 6.7 (b, c)**, respectively.

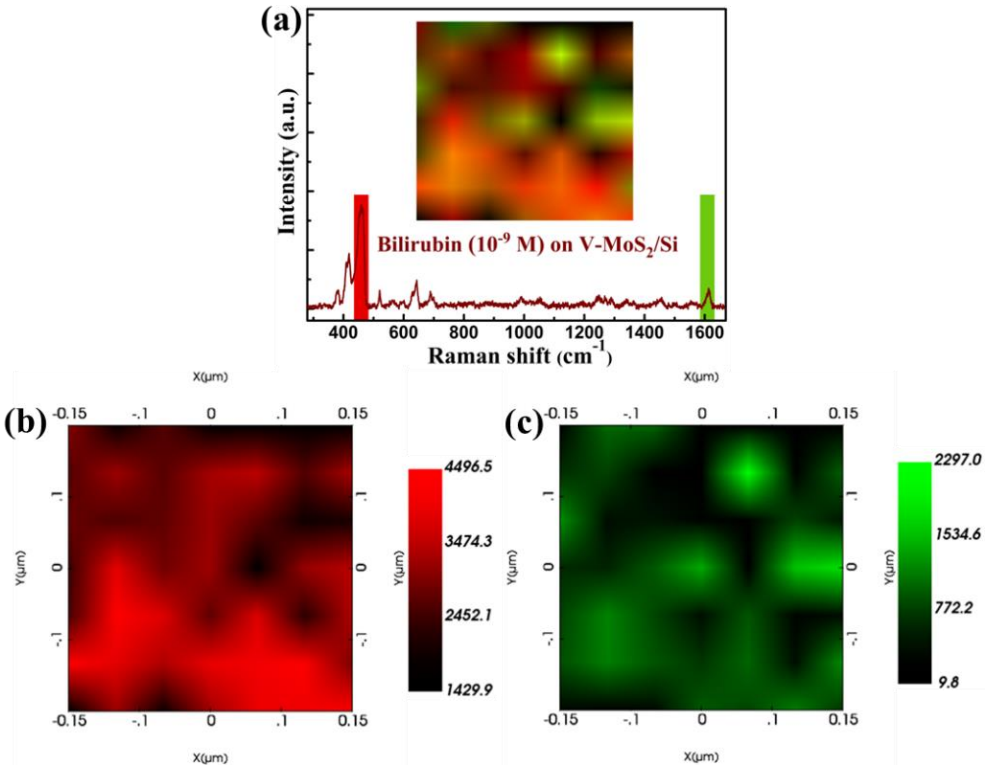

Figure 6.7 *(a) SERS spectrum and mapping of (b) MoS_2 (~457 cm^{-1}, shown by red color) and (c) bilirubin (~1612 cm^{-1}, shown by green color) on V-MoS_2/Si. Inset of (a) shows the SERS mapping of bilirubin adsorbed over V-MoS_2/Si.*

(iii) SERS Mapping of Bilirubin on V-MoS_2/SiO_2-Si SERS Substrate

Similarly, **Figure 6.8 (a)** and its inset illustrates the SERS spectrum and mapping of 10^{-7} M bilirubin adsorbed over V-MoS_2/SiO_2-Si SERS substrate. The inset particularly highlights a homogeneous distribution of bilirubin biomolecule adsorbed over V-MoS_2/SiO_2-Si SERS substrate. **Figure 6.8 (b, c)** shows the distinctive SERS peaks associated with MoS_2 at ~457 cm^{-1} (depicted in red) and bilirubin at ~1611 cm^{-1} (represented in green), respectively.

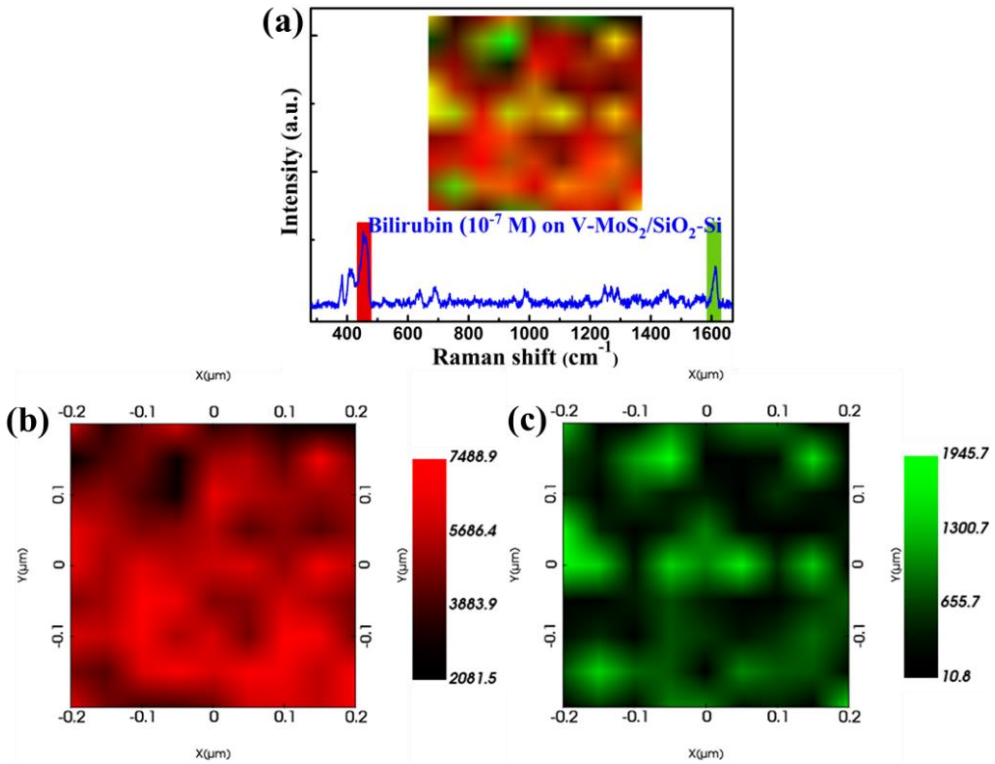

Figure 6.8 *(a) SERS spectrum and mapping of (b) MoS_2 (~457 cm^{-1}, shown by red color) and (c) bilirubin (~1611 cm^{-1}, shown by green color) on V-MoS_2/SiO_2-Si. Inset of (a) shows the SERS mapping of bilirubin adsorbed over V-MoS_2/SiO_2-Si.*

(iv) SERS Mapping of Bilirubin on H-MoS_2/SiO_2-Si SERS Substrate

Similarly, **Figure 6.9 (a)** and its inset display the SERS spectrum and mapping of 10^{-6} M bilirubin adsorbed over H-MoS_2/SiO_2-Si SERS substrate. Notably, the inset shows the uniform distribution of the bilirubin biomolecule adsorbed over H-MoS_2/SiO_2-Si SERS substrate. Additionally, **Figure 6.9 (b, c)** distinctly indicate the SERS peaks associated with MoS_2 at ~457 cm^{-1} (highlighted in red) and bilirubin at ~1613 cm^{-1} (depicted in green).

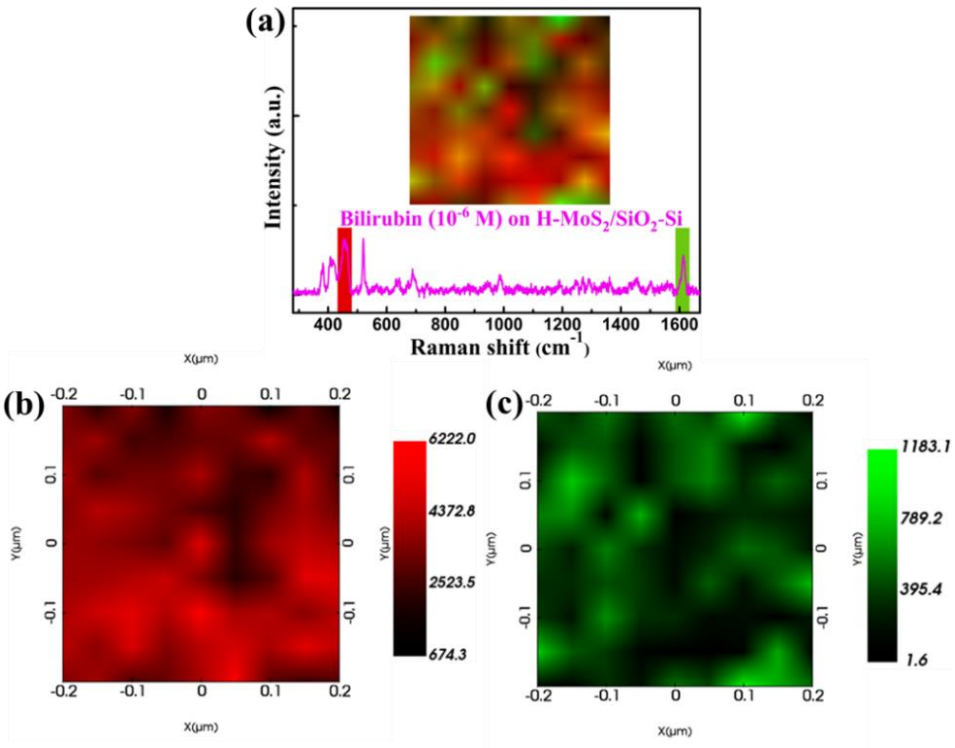

Figure 6.9 *(a) SERS spectrum and mapping of (b) MoS_2 (~457 cm^{-1}, shown by red color) and (c) bilirubin (~1613 cm^{-1}, shown by green color) on H-MoS_2/SiO_2-Si. Inset of (a) shows the SERS mapping of bilirubin adsorbed over H-MoS_2/SiO_2-Si.*

6.3.4 SERS Application for the Detection of Vitamin B_{12} using Different Prepared MoS_2 Nanostructures

Similarly, we performed the SERS study of vitamin B_{12} on different SERS substrates. The SERS signal for vitamin B_{12} on all synthesized substrates are shown in **Figure 6.10 (a-d)**. The significant SERS peak shift and enhanced intensity of vitamin B_{12} modes indicates the better adsorption of vitamin B_{12} on different SERS substrates showing strong semiconductor-biomolecule interaction. We observe that the SERS intensity decreases as the vitamin B_{12} concentration decreases. The limit of detection for vitamin B_{12} adsorbed on H-MoS_2/FTO (**Figure 6.10 (a)**), on V-MoS_2/Si (**Figure 6.10 (b)**), on V-MoS_2/SiO_2-Si (**Figure 6.10 (c)**) and on H-MoS_2/SiO_2-Si (**Figure 6.10 (d)**) are found to be 10^{-8}, 10^{-8}, 10^{-7} and 10^{-6} M, respectively, showing good SERS activity at room temperature. The most intense peak centred at ~1500 cm^{-1} (assigned to the stretching of C=C and C=N bonds of the corrin ring with some contributions from CH, CH_2 and CH_3 bending modes) is chosen here for the detection of vitamin B_{12}. The

linear variation of peak intensity at ~1500 cm^{-1} with vitamin B_{12} concentration on H-MoS_2/FTO, V-MoS_2/Si, V-MoS_2/SiO_2-Si and H-MoS_2/SiO_2-Si are displayed in **Figure 6.10 (e)**. The significant intensity of the SERS peak even at ten nanomolar (10^{-8} M) concentration of vitamin B_{12} on H-MoS_2/FTO and V-MoS_2/Si, indicates the ultrasensitive detection limit of these substrates, better than the other two substrates (V-MoS_2/SiO_2-Si and H-MoS_2/SiO_2-Si).

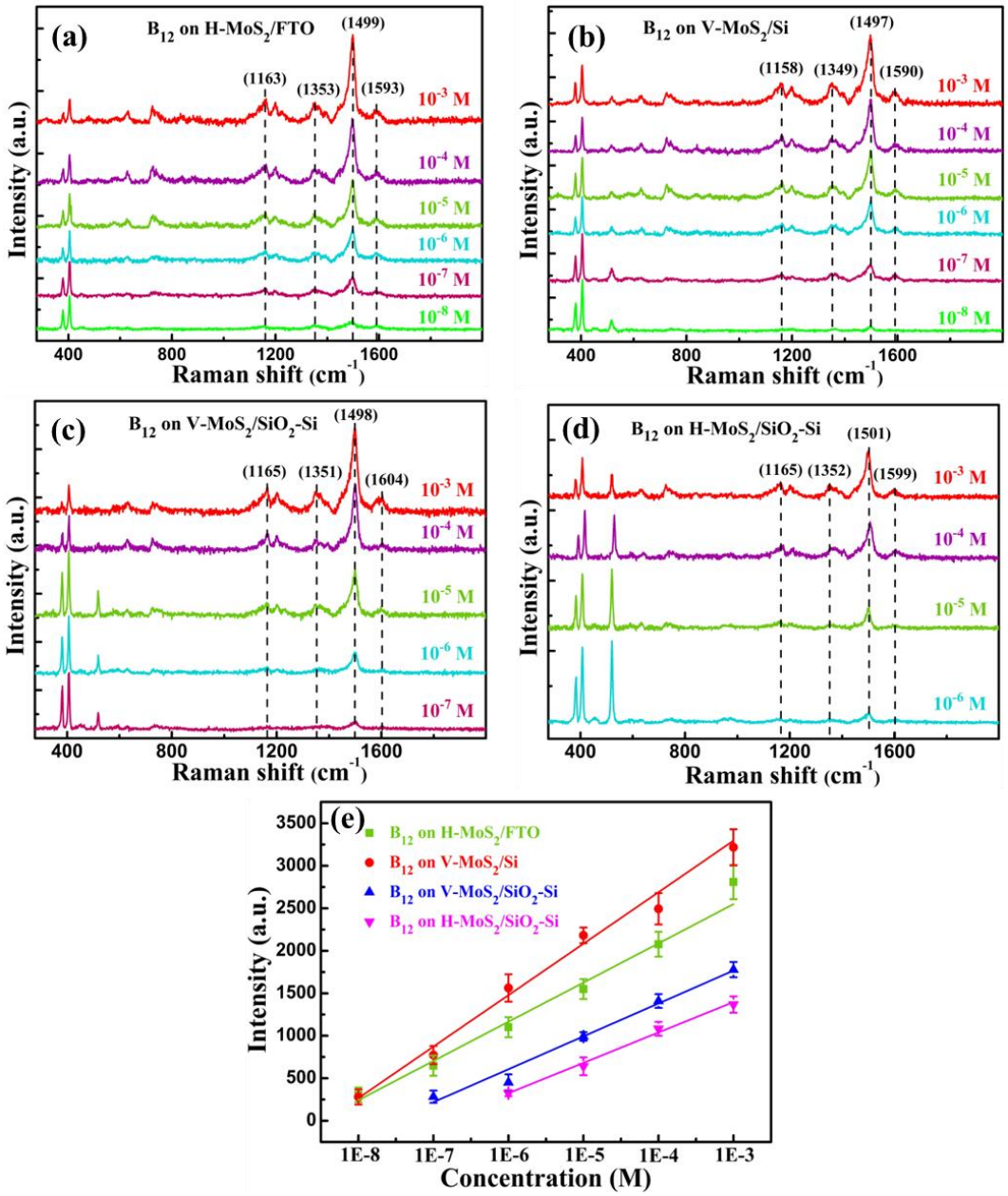

Figure 6.10 *SERS spectra of vitamin B_{12} at different concentrations on (a) H-MoS_2/FTO (10^{-3} to 10^{-8} M), (b) V-MoS_2/Si (10^{-3} to 10^{-8} M), (c) V-MoS_2/SiO_2-Si (10^{-3} to 10^{-7} M) and (d) H-MoS_2/SiO_2-Si (10^{-3} to 10^{-6} M). (e) Raman intensity of characteristic peak versus vitamin B_{12} concentrations on these substrates.*

The SERS mapping of vitamin B_{12} of different concentrations (10^{-6} M for H-MoS_2/FTO and V-MoS_2/Si, 10^{-5} M for V-MoS_2/SiO_2-Si and 10^{-4} M for H-MoS_2/SiO_2-Si) are shown in **Figure 6.11** to **Figure 6.14**, respectively.

(i) SERS Mapping of Vitamin B_{12} on H-MoS_2/FTO SERS Substrate

The SERS spectrum and mapping of 10^{-6} M vitamin B_{12} adsorbed over H-MoS_2/FTO SERS substrate are shown in **Figure 6.11 (a)** and inset, respectively. The SERS peak of MoS_2 at ~406 cm^{-1} and of vitamin B_{12} at ~1499 cm^{-1} are shown by red and green color in **Figure 6.11 (b, c)**, respectively. This clearly indicates the uniform distribution of vitamin B_{12} biomolecule adsorbed over H-MoS_2/FTO SERS substrate.

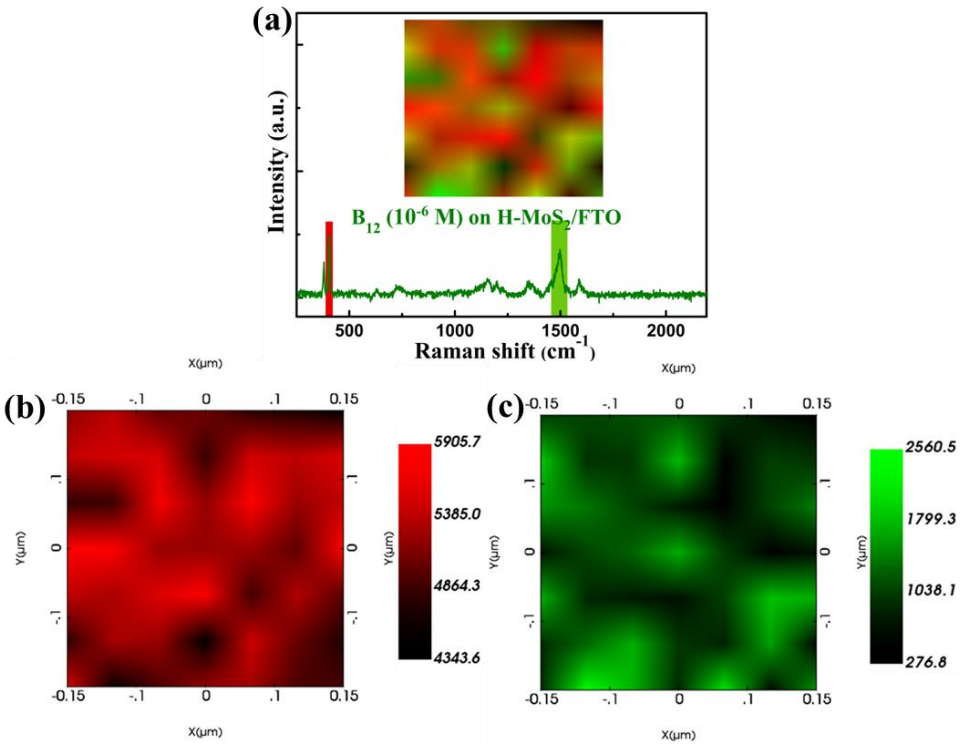

Figure 6.11 *(a) SERS spectrum and mapping of (b) MoS_2 (~406 cm^{-1}, shown by red color) and (c) vitamin B_{12} (~1499 cm^{-1}, shown by green color) on H-MoS_2/FTO. Inset of (a) shows the SERS mapping of vitamin B_{12} adsorbed over H-MoS_2/FTO.*

(ii) SERS Mapping of Vitamin B_{12} on V-MoS_2/Si SERS Substrate

Similarly, the SERS spectrum and mapping of 10^{-6} M vitamin B_{12} adsorbed over V-MoS_2/Si SERS substrate are shown in **Figure 6.12 (a)** and inset, respectively, indicating

uniform distribution of vitamin B_{12} biomolecule adsorbed over V-MoS_2/Si SERS substrate. The SERS peak of MoS_2 at ~406 cm^{-1} and of vitamin B_{12} at ~1497 cm^{-1} are shown by red and green color in **Figure 6.12 (b, c)**, respectively.

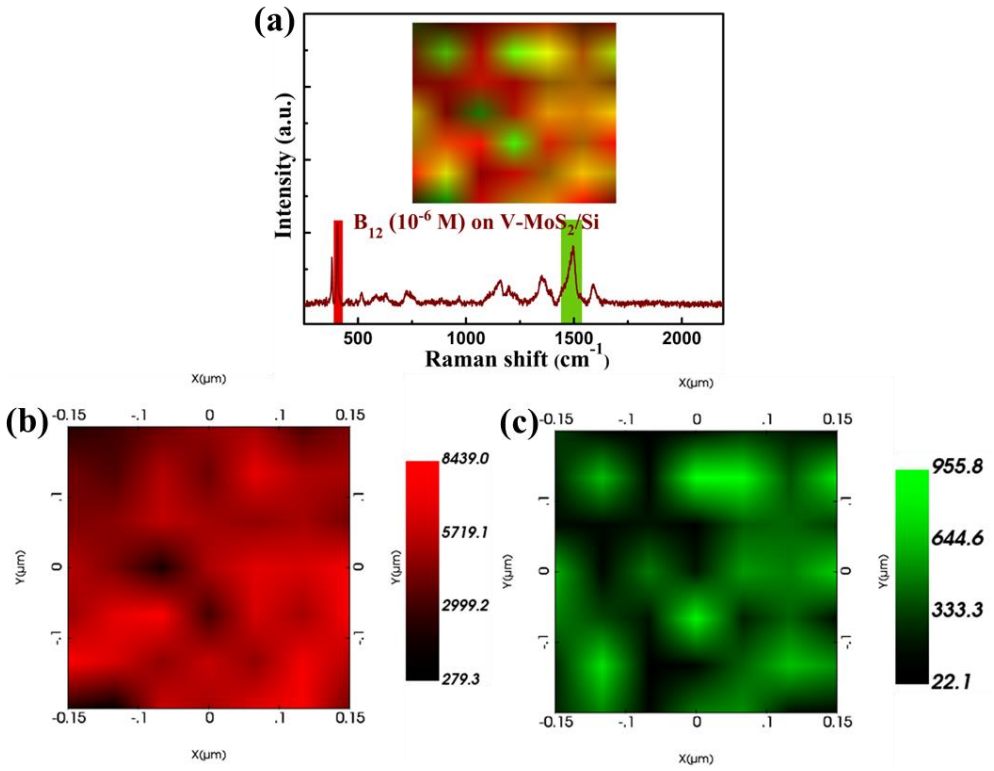

Figure 6.12 *(a) SERS spectrum and mapping of (b) MoS_2 (~406 cm^{-1}, shown by red color) and (c) vitamin B_{12} (~1497 cm^{-1}, shown by green color) on V-MoS_2/Si. Inset of (a) shows the SERS mapping of vitamin B_{12} adsorbed over V-MoS_2/Si.*

(iii) SERS Mapping of Vitamin B_{12} on V-MoS_2/SiO_2-Si SERS Substrate

Similarly, **Figure 6.13 (a)** and inset illustrates the SERS spectrum and mapping of 10^{-5} M vitamin B_{12} adsorbed over V-MoS_2/SiO_2-Si SERS substrate. The inset particularly highlights a homogeneous distribution of vitamin B_{12} biomolecule adsorbed over V-MoS_2/SiO_2-Si SERS substrate. **Figure 6.13 (b, c)** shows the distinctive SERS peaks associated with MoS_2 at ~406 cm^{-1} (depicted in red) and vitamin B_{12} at ~1498 cm^{-1} (represented in green), respectively.

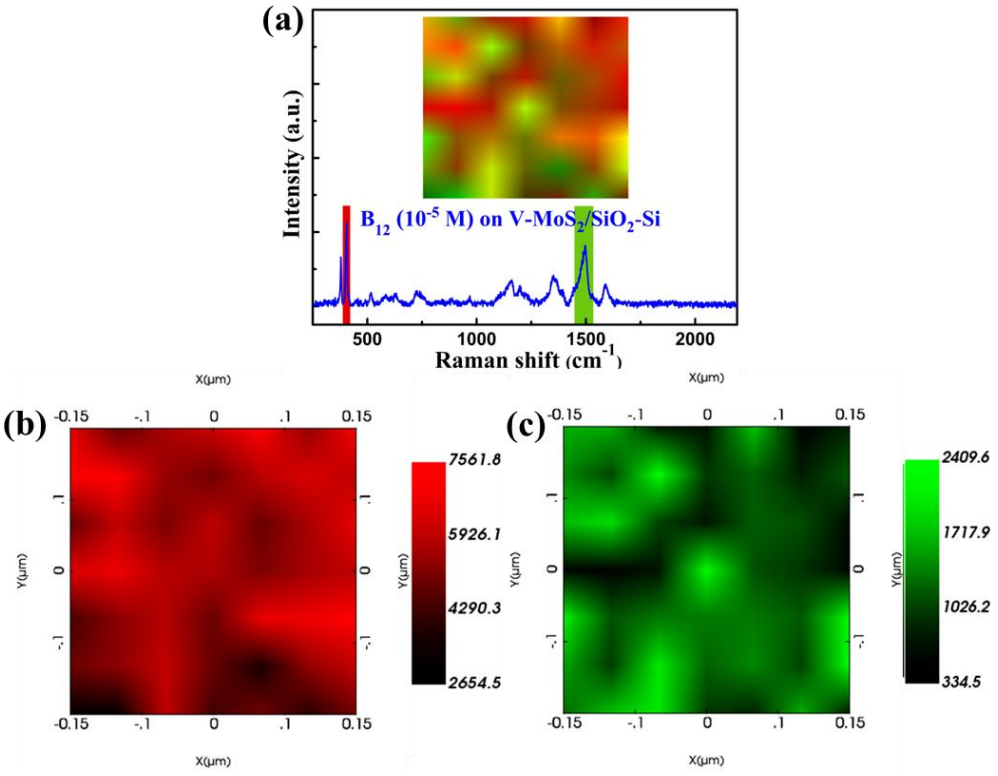

Figure 6.13 *(a) SERS spectrum and mapping of (b) MoS_2 (~406 cm^{-1}, shown by red color) and (c) vitamin B_{12} (~1498 cm^{-1}, shown by green color) on V-MoS_2/SiO_2-Si. Inset of (a) shows the SERS mapping of vitamin B_{12} adsorbed over V-MoS_2/SiO_2-Si.*

(iv) SERS Mapping of Vitamin B_{12} on H-MoS_2/SiO_2-Si SERS Substrate

Similarly, **Figure 6.14 (a)** and inset display the SERS spectrum and mapping of 10^{-4} M vitamin B_{12} adsorbed over H-MoS_2/SiO_2-Si SERS substrate. Notably, the inset shows the uniform distribution of the vitamin B_{12} biomolecule adsorbed over H-MoS_2/SiO_2-Si SERS substrate. Additionally, **Figure 6.14 (b, c)** distinctly indicate the SERS peaks associated with MoS_2 at ~406 cm^{-1} (highlighted in red) and bilirubin at ~1501 cm^{-1} (depicted in green).

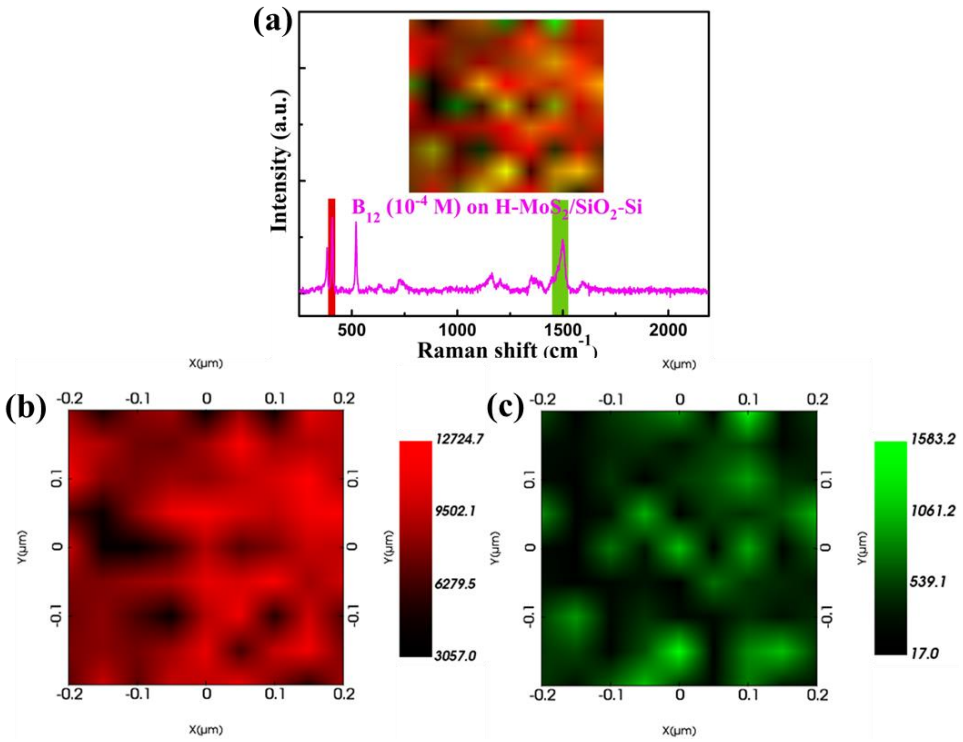

Figure 6.14 *(a) SERS spectrum and mapping of (b) MoS_2 (~406 cm^{-1}, shown by red color) and (c) vitamin B_{12} (~1501 cm^{-1}, shown by green color) on H-MoS_2/SiO_2-Si. Inset of (a) shows the SERS mapping of vitamin B_{12} adsorbed over H-MoS_2/SiO_2-Si.*

6.3.5 SERS Mechanism for Biomolecules Detection using MoS_2 Substrates

SERS signal on MoS_2 can be ascribed to the Herzberg-Teller vibronic coupling of various resonances in the biomolecule-nanostructure system, that comprises of three main processes: (i) interfacial ground-state charge transfer (μ_{GSCT}) that is associated with the chemical interaction between the biomolecule and the nanostructure in the ground state without excitations (ii) photoinduced charge transfer (μ_{PICT}) resonance that is featured by the charge transfer between the biomolecule and the substrate in resonance with excitations (iii) electronic excitation resonance that occurs when excitation frequency coincides with the molecular transition resulting in resonance Raman scattering (RRS) within the molecule itself [224, 225]. All these three processes contribute to the A, B and C terms that combinedly alters the electron density distribution of biomolecules, ensuing greater polarizability and hence efficient SERS detection. Thus, the polarizability (α) of the molecule is expressed as [226]-

$$\alpha_{\sigma\rho} = A + B + C \qquad (6.1)$$

The A-term is responsible for RRS, following Franck-Condon selection rules and allows only totally symmetric Raman modes. The B- and C-term are believed to borrow the intensity from nearby allowed molecular or exciton transition via Herzberg-Teller coupling constant (h) and enhances both totally and non-totally symmetric Raman modes. **Figure 6.15** shows the schematic of the coupling scheme for the B- and C-term. The Raman transition intensity (I) is obtained from the polarizability tensor as follows [99, 225] -

$$I = [8\pi (\omega \pm \omega_{I'I})^4 I_L/9c^4] \sum \alpha_{\sigma\rho}{}^2 \quad (6.2)$$

where I_L is the intensity of the incident laser at ω and $\omega_{I'I}$ is the molecular transition frequency between states I and I′.

The A- term in **equation 6.1** is given by-

$$R_{IC}(\omega) = \frac{\mu_{IC}\mu_{IC}\langle i|k\rangle\langle k|f\rangle}{((\varepsilon_1(\omega)+2\varepsilon_0)^2+\varepsilon_2^2(\omega))\,((\omega_{IC}{}^2-\omega^2)+\gamma_{IC}^2)} \quad (6.3)$$

where μ_{IC} is a CT transition from the HOMO level of molecule to the CB edge (at $\omega = \omega_{IC}$). ε_0 is the permittivity of the surrounding and, ε_1 and ε_2 are the real and imaginary parts of the permittivity of the SERS substrate, respectively, γ is the damping factor related to each process. Similarly, A-term can be written as transition from VB edge to LUMO level of the molecule (at $\omega = \omega_{VK}$). For A-term, either of the one resonance is allowed. The B-term stems from the CT transition from the HOMO level of the molecule to the CB edge of the substrate and are coupled either to the molecular transitions (at $\omega = \omega_{IK}$) or exciton transition (at $\omega = \omega_{VC}$) by a Herzberg−Teller coupling term (h_{CK} or h_{IV}). This Herzberg−Teller vibronic coupling was initially introduced by Herzberg and Teller. It drives the SERS enhancement in semiconductor substrates by interconnecting molecular transitions with charge transfer transitions between biomolecule and SERS substrates. Thus, the B-term is given by-

$$R_{ICK}(\omega) = \frac{\mu_{IK}\,\mu_{IC}\,h_{CK}\langle i|Q_k|f\rangle}{((\varepsilon_1(\omega)+2\varepsilon_0)^2+\varepsilon_2^2(\omega))\,((\omega_{IC}^2-\omega^2)+\gamma_{IC}^2)((\omega_{IK}^2-\omega^2)+\gamma_{IK}^2)} \quad (6.4)$$

$$R_{ICV}(\omega) = \frac{\mu_{VC}\,\mu_{IC}\,h_{IV}\langle i|Q_k|f\rangle}{((\varepsilon_1(\omega)+2\varepsilon_0)^2+\varepsilon_2^2(\omega))\,((\omega_{IC}^2-\omega^2)+\gamma_{IC}^2)((\omega_{VC}^2-\omega^2)+\gamma_{VC}^2)} \quad (6.5)$$

where μ_{IK} and μ_{VC} are the moment related to molecular and exciton transition, respectively. and ⟨i|Qk|f⟩ is the vibrational selection rule that allows different modes. Similarly, the C-term is obtained from the CT from VB of the substrate to the LUMO level of the biomolecule and are coupled either to the molecular transitions (at $\omega = \omega_{IK}$) or exciton transition (at $\omega = \omega_{VC}$) via h_{IV} or h_{CK}.

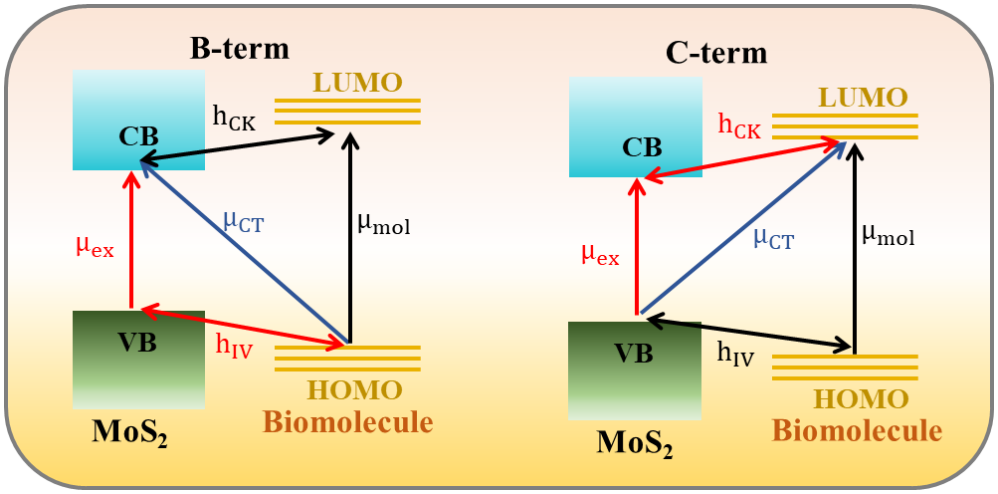

Figure 6.15 *Schematic of the coupling scheme for the B-term: CT resonance is coupled with molecular resonance or exciton resonance via h_{CK} or h_{IV}, and, C-term: CT resonance is coupled with molecular resonance or exciton resonance via h_{IV} or h_{CK}.*

The CT mechanism between analyte biomolecule and SERS substrate are also affected by the electrical properties of the underlying substrate and its electronic coupling with MoS_2 [220]. Different underlying substrates modulates the electrical properties of MoS_2 due to different surface potential [220]. The FTO exhibits good transparency with large band-gap (E_g > 3 eV) and low electrical resistivity owed to increased carrier concentrations arising from oxygen vacancies and fluorine substitution [227]. In case of H-MoS_2 grown over FTO coated glass substrate, the work function of FTO (~4.0 eV) is expected to lie above the CB edge of MoS_2 (the CB edge, Fermi energy and VB edge are at energies of ~4.4, ~4.7 and ~5.8 eV below the vacuum level), as per literature reports [228-231]. Under light illumination, this alignment facilitates the movement of electrons from the FTO substrate to MoS_2, thus shifting the fermi level of MoS_2 upward and electron concentration increases in the CB of MoS_2, as shown

schematically in **Figure 6.16**. This high electron injection in the MoS_2 region and holes at the FTO side, results in n-type doping of MoS_2 in H-MoS_2/FTO, which provides larger number of electrons in the CB of MoS_2 to facilitate the enhanced charge transfer with adsorbed biomolecules and hence better SERS activity of H-MoS_2/FTO.

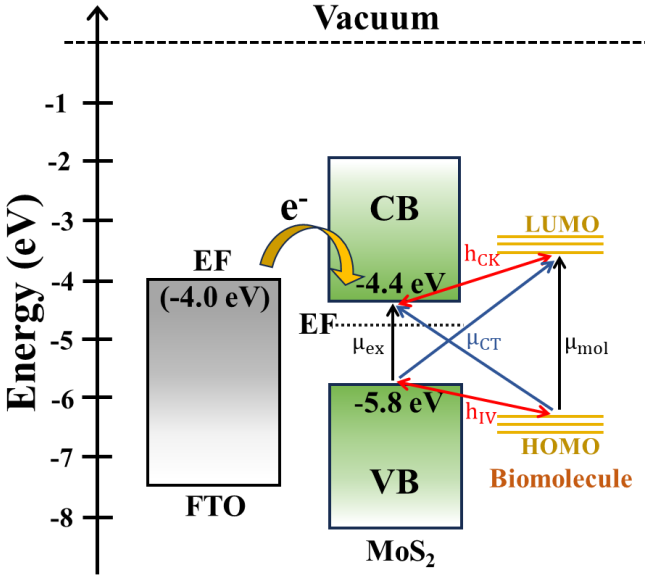

Figure 6.16 *Schematic energy band diagram for charge transfer among FTO, H-MoS_2 and biomolecule.*

The high SERS performance of V-MoS_2/Si is mainly contributed by the vertical morphology leading to better light trapping and adsorption of analyte biomolecule. The vertical morphology enhances light capture capability via multiple reflection, absorption and scattering of the incident light within the freestanding MoS_2 nanoflakes, that results in enhanced photo absorption within the structure [99, 232]. The light absorption behavior of different MoS_2 nanostructures grown over different substrates have been observed using UV-vis absorption measurement, as shown in **Figure 2.17** of **chapter 2**. Two signature absorption peaks (A exciton and B exciton), around ~677 and ~626 nm, are observed for MoS_2 grown over different substrates and originates from direct excitonic transitions from the spin-orbital splitting of VB to the minimum of CB. The spectra also show a broad peak in the range of ~400-600 nm, referring to electron transition between the higher density of state regions. The absorption

spectra also clearly reveal that the vertical morphology of MoS_2 films shows higher absorbance at the wavelength of excitation source (532 and 633 nm) compared to horizontal grown films of MoS_2, which can further improve the light capture capacity, that leads to better SERS activity.

The dielectric SiO_2 substrate possess dangling bonds that serve as charge defects and impurities leading to electron transfer between SiO_2 and MoS_2. Additionally, the polar behavior of SiO_2 results in extrinsic scattering. These combined effects limit the electron transfer between MoS_2 and probe biomolecules, resulting in a lower detection limit for MoS_2 films grown over SiO_2-Si substrate [233]. Thus, the rough surface of H-MoS_2 grown on FTO substrate and the highly dense edge enriched V-MoS_2 nanostructure grown on Si substrate provides better surface wettability that ensures good biomolecule adsorption and improves the light absorption and trapping capability, showing better enhancement in SERS signal of biomolecules. To further analyse the CT mechanism, we examined the change in the room temperature PL spectrum of different substrates with and without vitamin B_{12} biomolecules. For bilirubin biomolecule, the room temperature PL and its quenching was difficult to observe with a low power laser, while high power may lead to biomolecule degradation. Hence, we observe this phenomenon only for vitamin B_{12} biomolecule. **Figure 6.17** clearly shows that the PL intensity of H-MoS_2/FTO, V-MoS_2/Si, V-MoS_2/SiO_2-Si and H-MoS_2/SiO_2-Si with vitamin B_{12} biomolecule (10^{-3} M) is reduced significantly in comparison with the PL intensity of respective SERS substrates without vitamin B_{12}. This indicates that maximum electrons are transferred from SERS substrate to vitamin B_{12} biomolecules and fewer electrons are jumped back from CB to VB, verifying CT process in vitamin B_{12} adsorbed over SERS substrates [234].

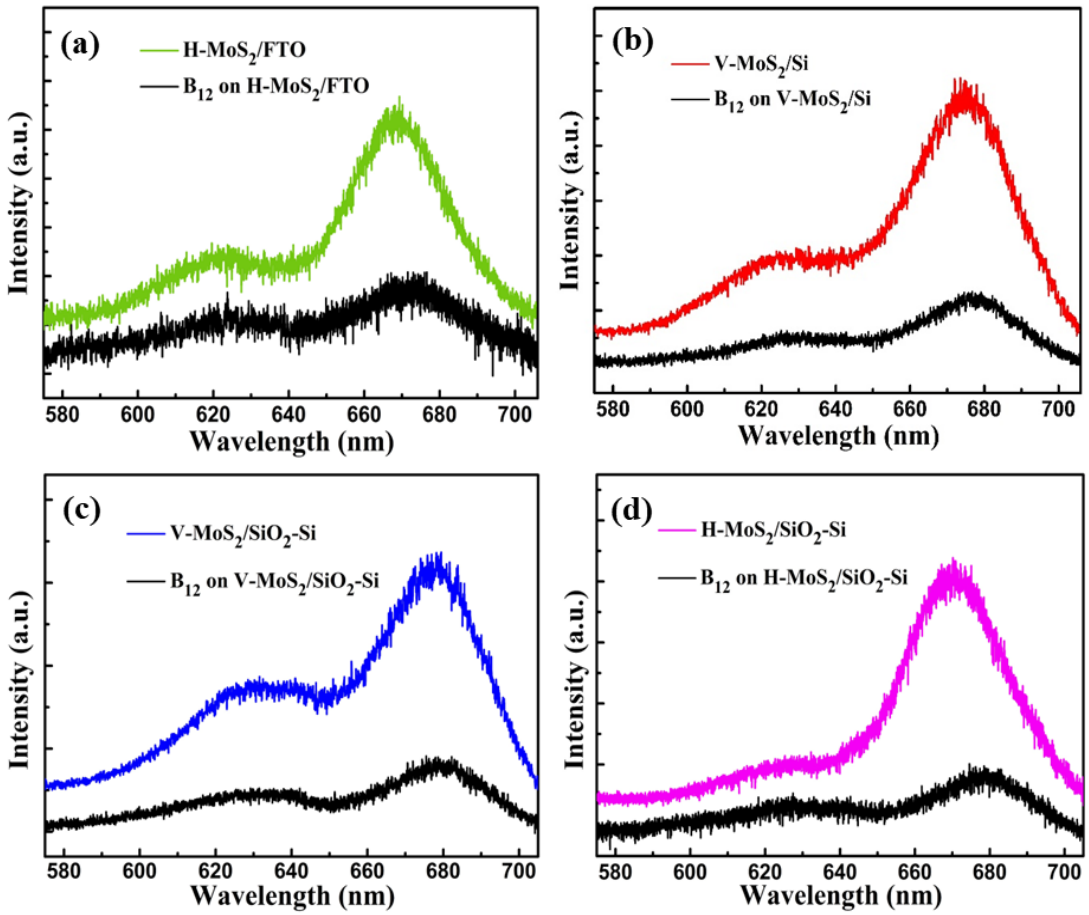

Figure 6.17 *The PL spectra of (a) H-MoS_2/FTO, (b) V-MoS_2/Si, (c) V-MoS_2/SiO_2-Si and (d) H-MoS_2/SiO_2-Si SERS substrates with and without vitamin B_{12}.*

6.3.6 Calculation of Number of Biomolecules Probed in SERS (N_{SERS}) and Estimation of SERS Enhancement Factor (EF)

Enhancement Factor (EF) refers to the amplification of Raman signals that occurs when molecules are adsorbed onto the SERS substrate. Here, we estimate the SERS enhancement factor by choosing ~1613 cm^{-1} peak for bilirubin and ~1500 cm^{-1} peak for vitamin B_{12} and calculate using the following equation [73, 235]-

$$EF = \frac{I_{SERS}}{N_{SERS}} \times \frac{N_{Raman}}{I_{Raman}} \qquad (6.6)$$

where I_{SERS} and I_{Raman} denotes the intensity of SERS peaks (~1613 cm^{-1} for bilirubin and ~1500 cm^{-1} for vitamin B_{12}) on SERS-active substrate and normal Raman intensity of

biomolecule on bare substrates, respectively. The I_{Raman} for bilirubin and vitamin B_{12} over different underlying substrates are noted from **Figure 6.18** and listed in **Table 6.3**.

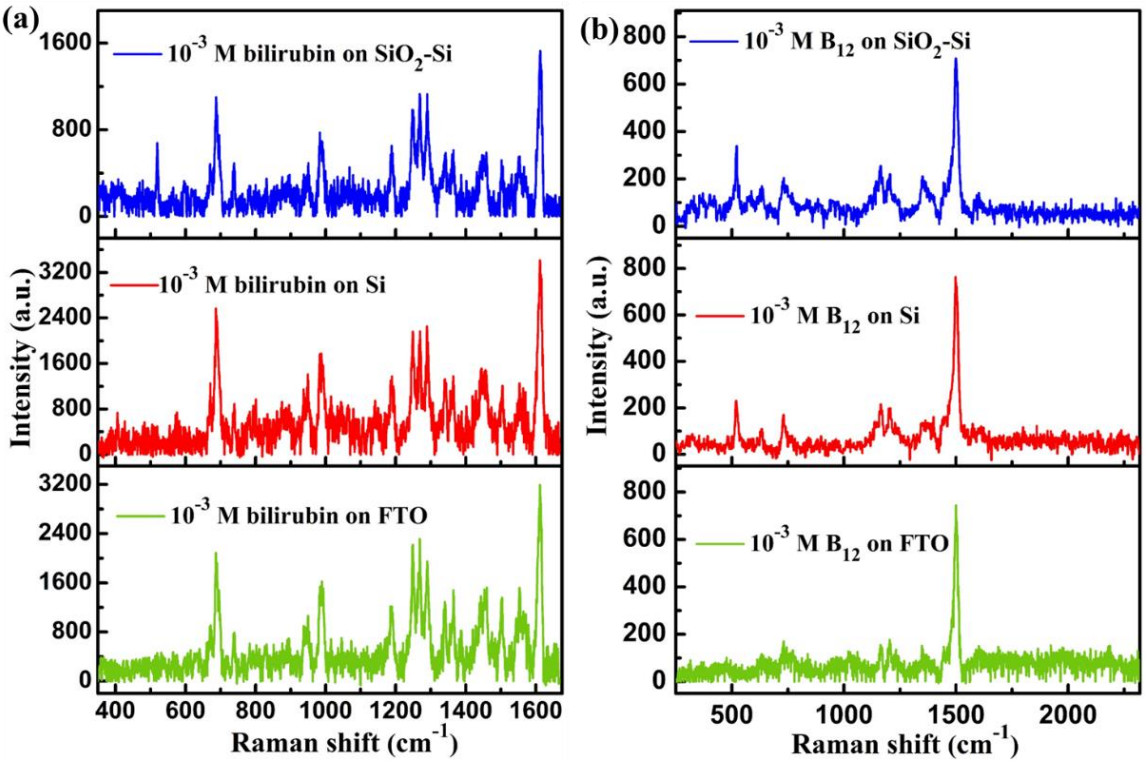

Figure 6.18 *Raman spectra of 10^{-3} M concentration of (a) bilirubin and (b) vitamin B_{12} over FTO coated glass, Si and SiO_2-Si substrate.*

Table 6.3 I_{Raman} and I_{SERS} for both the biomolecules on different substrates.

	I_{SERS}			**I_{Raman}**	
Substrates	**Bilirubin**	**Vitamin B_{12}**	**Substrates**	**Bilirubin**	**Vitamin B_{12}**
H-MoS_2/FTO	396	304	**FTO**	3143	784
V-MoS_2/Si	652	279	**Si**	3404	752
V-MoS_2/SiO_2-Si	549	282	**SiO_2-Si**	1528	699
H-MoS_2/SiO_2-Si	500	324			

The number of biomolecules probed for normal Raman scattering (N_{Raman}) is given by [73, 235]-

$$N_{Raman} = \frac{\rho h N_A A_{Raman}}{M} \quad (6.7)$$

where ρ and M are the density and molecular weight of the bulk biomolecule, h is the confocal depth of the laser into sample and N_A is the Avogadro constant.

For bilirubin: M = 584.67 g/mol and $\rho = 1.31$ g/cm^3

For vitamin B_{12}: M = 1355.38 g/mol and $\rho = 1.16$ g/cm^3

A_{Raman} is the laser spot area and is given by = ($\pi \times r^2$)

A_{sub} is the effective area of the substrate and is given by = ($\pi \times R^2$)

where spot size (r) and h of the laser for 50x objective lens are given by -

$$r = \frac{\lambda}{\pi \times \text{N.A.}}\, nm \quad \text{and} \quad h = \frac{2 \times \lambda}{(\text{N.A.})^2}\, nm \tag{6.8}$$

where λ and N.A. are the wavelength of the incident laser and the numerical aperture of the objective lens (0.8 for 50x objective lens), respectively.

For 532 nm laser, $r = \frac{532}{3.14 \times 0.8} = 0.2118$ μm and $h = \frac{2 \times 532}{0.8 \times 0.8} = 1.662$ μm

For 633 nm laser, $r = \frac{633}{3.14 \times 0.8} = 0.2520$ μm and $h = \frac{2 \times 633}{0.8 \times 0.8} = 1.978$ μm

R is the average circular radius of the lowest detected biomolecule dropped on SERS substrate, after drying and its obtained value for both the biomolecules on different SERS substrates are listed in **Table 6.4**.

Table 6.4 The values of R obtained on different SERS substrates.

	H-MoS_2/FTO (in μm)	V-MoS_2/Si (in μm)	V-MoS_2/SiO_2-Si (in μm)	H-MoS_2/SiO_2-Si (in μm)
Bilirubin	748.50	744.71	819.56	878.01
Vitamin B_{12}	966.20	921.88	1011.72	1077.43

Therefore,

For bilirubin biomolecules:

$$N_{Raman} = \frac{(1.31\ \text{g/cm}^3) \times (1.978\ \mu\text{m}) \times (6.023 \times 10^{23}\ \text{molecules/mol}) \times 3.14 \times (0.252\ \mu\text{m})^2}{584.67\ \text{g/mol}}$$

$$= 5.3 \times 10^8 \text{ molecules}$$

For vitamin B_{12} biomolecules:

$$N_{Raman} = \frac{(1.16\ g/cm^3) \times (1.662\ \mu m) \times (6.023 \times 10^{23}\ molecules/mol) \times 3.14 \times (0.212\ \mu m)^2}{1355.38\ g/mol}$$

$$= 1.2 \times 10^8 \text{ molecules}$$

The number of biomolecules probed in SERS (N_{SERS}) is given by [73, 235]-

$$N_{SERS} = \frac{CVN_A A_{Raman}}{A_{sub}} \quad (6.9)$$

where C is the molar concentration of the reference biomolecule in solution and V is the solution volume irradiated. Thus, N_{SERS} for bilirubin over H-MoS_2/FTO is-

$$N_{SERS} = \frac{(10^{-11}\ M) \times (2\ \mu L) \times (6.023 \times 10^{23} molecules/mol) \times 3.14 \times (0.252\ \mu m)^2}{3.14 \times (748.50\ \mu m)^2} = 1.37 \sim 1 \text{ molecule}$$

Number of molecules per $\mu m^2 = \frac{1.37\ molecules}{3.14 \times (0.252 \mu m)^2} \sim 7\ molecules/\mu m^2$

Similarly, we calculate number of molecules per μm^2 for other biomolecules over different substrates for lowest concentration and are listed in **Table 6.5**. It clearly shows that H-MoS_2/FTO and V-MoS_2/Si shows approximately 7 molecules per μm^2 at 10^{-11} M concentration for bilirubin indicating near single molecule detection.

Table 6.5 Calculated number of molecules per μm^2 (at lowest concentration) for bilirubin and vitamin B_{12} over different substrates at lowest concentration.

	H-MoS_2/FTO	**V-MoS_2/Si**	**V-MoS_2/SiO_2-Si**	**H-MoS_2/SiO_2-Si**
Bilirubin	~7 (10^{-11} M)	~7 (10^{-11} M)	~571 (10^{-9} M)	~4976 (10^{-8} M)
Vitamin B_{12}	~4109 (10^{-8} M)	~4514 (10^{-8} M)	~37480 (10^{-7} M)	~330467 (10^{-6} M)

Therefore, EF for bilirubin biomolecule over H-MoS_2/FTO is-

$$EF = \frac{396 \times 5.32 \times 10^8}{1.37 \times 3143} = 4.9 \times 10^7$$

Similarly, we calculate EF for other biomolecules on different substrates and the obtained values are listed in **Table 6.6**.

Table 6.6 EF for different biomolecules on different SERS substrates.

	H-MoS_2/FTO	**V-MoS_2/Si**	**V-MoS_2/SiO_2-Si**	**H-MoS_2/SiO_2-Si**
Bilirubin	4.9×10^7	7.4×10^7	1.7×10^6	1.7×10^5
Vitamin B_{12}	8.1×10^4	7.1×10^4	9.2×10^3	1.2×10^3

A comparison of SERS detection limit of both the biomolecules on different SERS substrate with previously reported works are given in **Table 6.7**. To the best of our knowledge, the detection limit in this work is considerably higher than previously reported values with pristine semiconducting substrate.

Table 6.7 Comparison of the SERS detection limit of bilirubin and vitamin B_{12} over different substrates with different analytical methods.

SERS Substrates	**Preparation Method**	**Detection Method**	**Analyte molecule**	**Detection Limit (M)**	**References**
Functionalized BN on Ag nanoarray	Ball milling stripping	SERS	Bilirubin	1.4×10^{-8}	Actuators B Chem., 2021, **334**, 1296342.[199]
MoS_2@ZnO @Ag	Hydrothermal	SERS	Bilirubin	10^{-8}	Appl. Surf. Sci., 2022, **598**, 153750.[73]
Ag@Fe_2O_3	Hydrothermal	SERS	Bilirubin	2.3×10^{-8}	Appl. Surf. Sci., 2021, **542**, 148757.[236]
Carbon dots	Hydrothermal	Fluorescence assay	B_{12}	0.1×10^{-6}	Light Sci. Appl., 2020, **9**, 117.[237]
Ag-deposited TiO_2 nanotube	Anodization	SERS	B_{12}	2.48×10^{-8}	Microchem. J., 2022, **181**, 107813.[238]
H-MoS_2/FTO & V-MoS_2/Si	CVD	SERS	Bilirubin	10^{-11}	**Present work**
H-MoS_2/FTO & V-MoS_2/Si	CVD	SERS	B_{12}	10^{-8}	**Present work**

6.3.7 Temperature-Dependent SERS Measurements

The Photoinduced Charge Transfer (PICT) process is a wavelength dependent phenomenon that is associated with photo-induced electron transfer (originated from the separation of excitons) between substrate and molecule in resonance with the excitation photons. However, the separation of excitons is suppressed via non-radiative recombination originating from the lattice thermal vibration, thus deteriorating the PICT efficiency. Low temperature condition can serve as a promising strategy that decreases the phonon generation by weakening the lattice thermal vibration. Hence, thereby declining the non-radiative recombination rate and allowing more photo-induced electrons to take part in PICT process. As discussed in **chapter 3**, the enhanced PL intensity at low temperature compared to the room temperature, clearly demonstrates that the photo-induced electron density increases largely because of effectively decline of non-radiative recombination at low temperature. This will promote the charge transfer from SERS substrate to biomolecule under light illumination, proposing a useful approach for facilitating PICT transitions and amplifying the Raman scattering cross-section. To explore the mechanism of highly efficient PICT transition at low-temperature between the SERS-active substrate and analyte biomolecules, temperature-dependent SERS at low temperatures from 323 K to 80 K were performed for both the biomolecules on all prepared SERS substrates. The low temperature SERS significantly promotes the electron transfer from the substrate to molecular excited states in PICT process, resulting in enhanced SERS activity of MoS_2 nanostructures at low temperatures. We demonstrate this exotic phenomenon by performing the temperature-dependent SERS of bilirubin and vitamin B_{12} on all prepared SERS substrates under a fixed laser power. **Figure 6.19 (a, b)** shows the temperature-dependent SERS of 10^{-9} M bilirubin on H-MoS_2/FTO, while **Figure 6.19 (c, d)** shows the temperature-dependent SERS of 10^{-9} M bilirubin on V-MoS_2/Si. **Figure 6.19 (e, f)** shows the temperature-dependent SERS of 10^{-7} M bilirubin on V-

MoS_2/SiO_2-Si, while **Figure 6.19 (g, h)** shows the temperature-dependent SERS of 10^{-6} M bilirubin on H-MoS_2/SiO_2-Si. Similarly, **Figure 6.20 (a, b)** shows the temperature-dependent SERS for 10^{-6} M vitamin B_{12} on H-MoS_2/FTO, while **Figure 6.20 (c, d)** shows the temperature-dependent SERS for 10^{-6} M vitamin B_{12} on V-MoS_2/Si**. Figure 6.20 (e, f)** shows the temperature-dependent SERS for 10^{-5} M vitamin B_{12} on V-MoS_2/ SiO_2-Si, while **Figure 6.20 (g, h)** shows the temperature-dependent SERS for 10^{-4} M vitamin B_{12} on H-MoS_2/SiO_2-Si. The spectra clearly show that the SERS intensities of bilirubin and vitamin B_{12} on different SERS substrates gradually increases with decreasing temperature. The linear fitting of Raman intensity of the characteristic peaks of bilirubin (~1613 cm^{-1}) and vitamin B_{12} (~1500 cm^{-1}) versus temperature on different SERS substrates are shown in **Figure 6.21 (a, b)**, respectively. It clearly shows the boost in the SERS vibrational signal of both the biomolecules on different SERS substrate with decreasing temperature. For a semiconductor substrate, SERS enhancement (I_{Raman}) depends on the Raman scattering cross section (σ_{ads}^{R}) of the adsorbed biomolecule: $I_{Raman} \propto \sigma_{ads}^{R}$. At low temperature, the excited electron density increases largely because of decreased non-radiative recombination. This facilitates the PICT transition from the SERS substrate to the analyte biomolecule and enhances the Raman scattering cross section (σ_{ads}^{R}), giving significant SERS enhancement (I_{Raman}) as described in **equation 6.11** [239]-

$$\sigma_{ads}^{R} \propto \frac{N_0}{1+\left(\frac{\tau}{\tau_0}\right)e^{-\frac{E_A}{kT}}} \propto N_0 e^{\frac{E_A}{kT}} \tag{6.10}$$

$$I_{Raman} \propto 1/T \tag{6.11}$$

where, N_0 is the number of electrons at 0 K, τ is the exciton lifetime, τ_0 is the effective scattering time, E_A is the activation energy, k is the Boltzmann constant and T is the temperature in K. Thus, we observe the significant enhancement in the SERS signal with the decrease of temperature due to large number of electrons transferred from the CB of SERS-active substrate to the LUMO level of biomolecules.

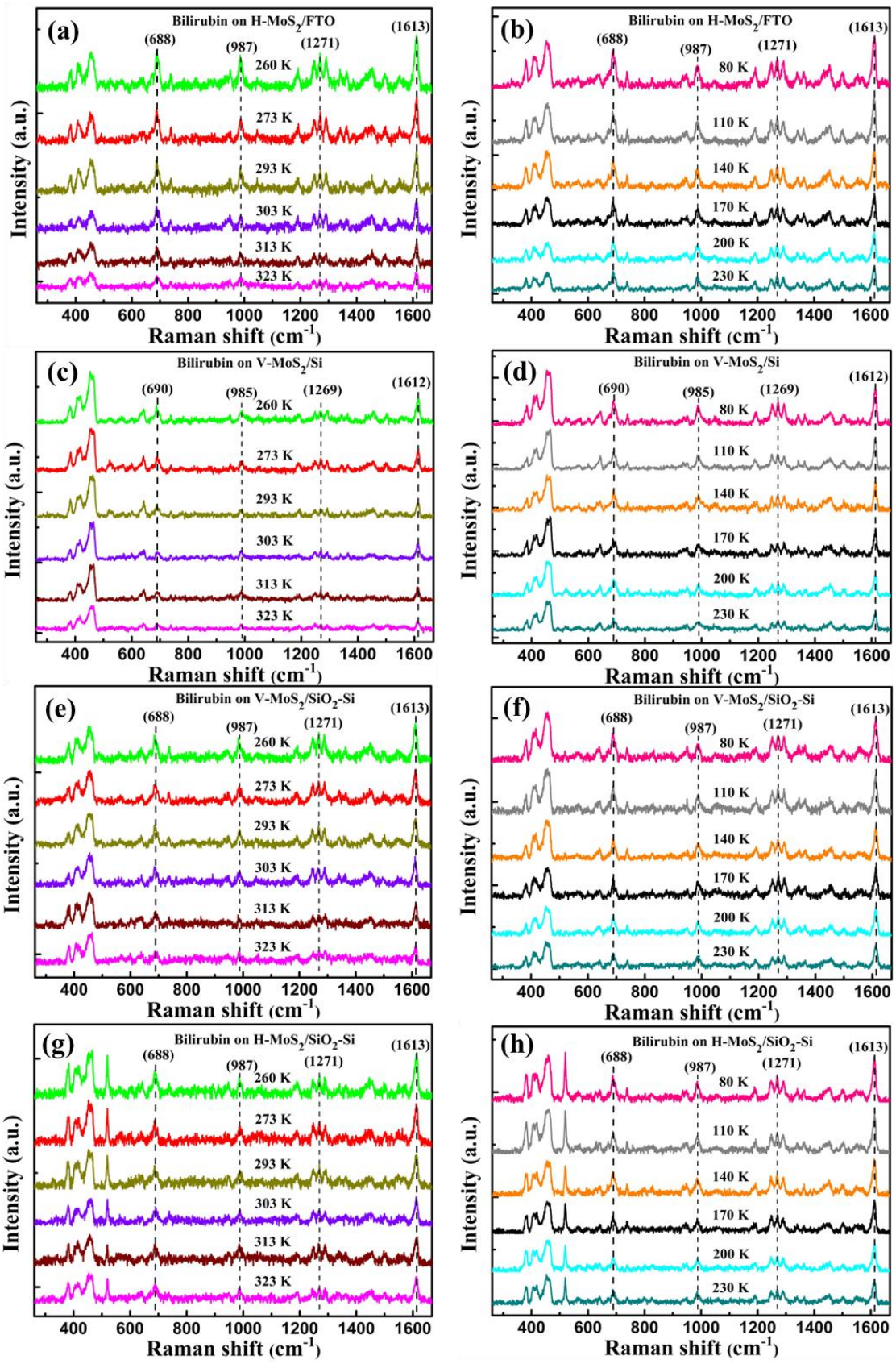

Figure 6.19 *Temperature-dependent SERS from 323 to 260 K and from 230 to 80 K of (a, b) 10^{-9} M bilirubin on H-MoS_2/FTO, (c, d) 10^{-9} M bilirubin on V-MoS_2/Si, (e, f) 10^{-7} M bilirubin on V-MoS_2/SiO_2-Si and (g, h) 10^{-6} M bilirubin on H-MoS_2/SiO_2-Si.*

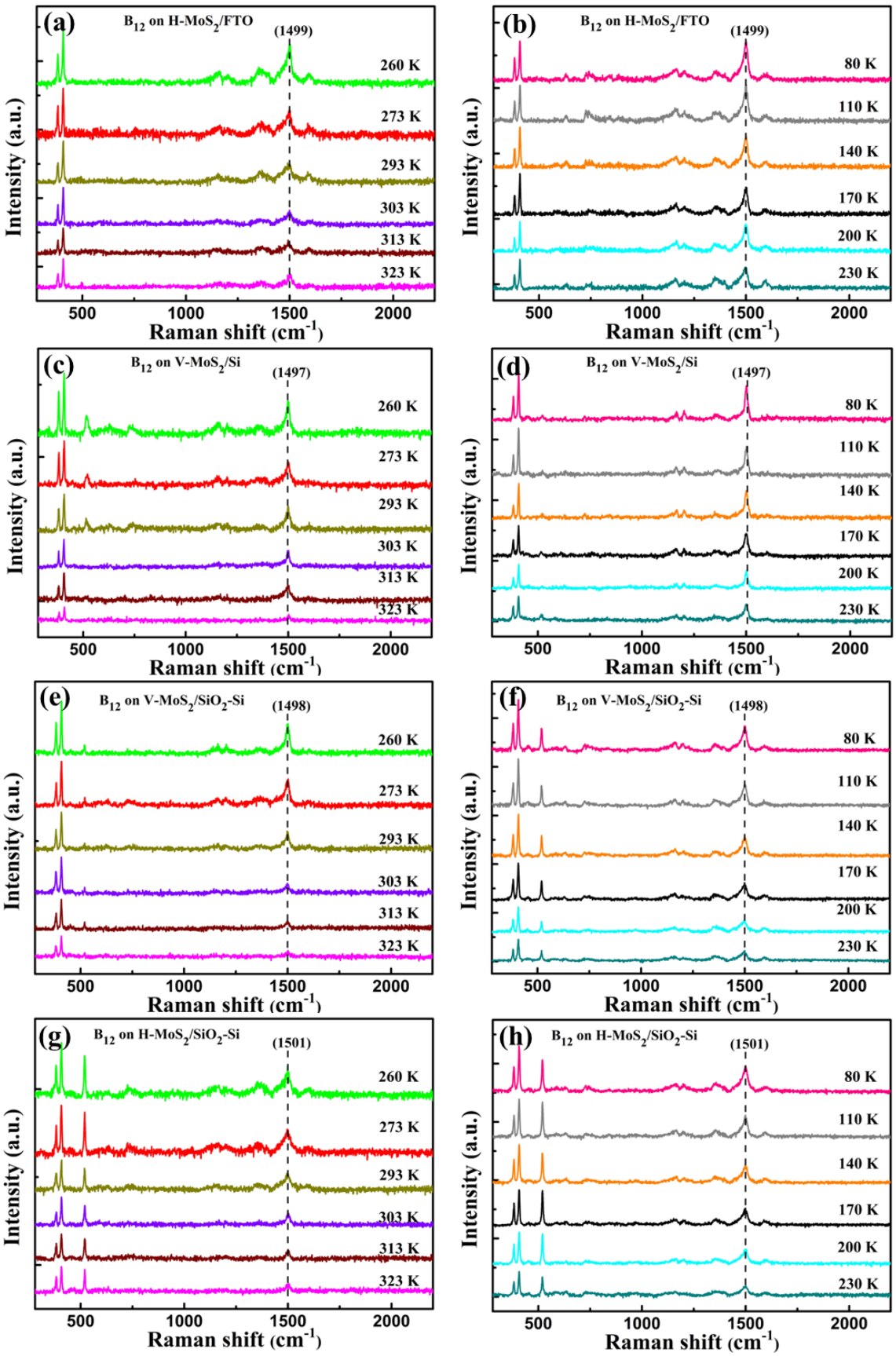

Figure 6.20 *Temperature-dependent SERS from 323 to 260 K and from 230 to 80 K of (a, b) 10^{-6} M vitamin B_{12} on H-MoS_2/FTO, (c, d) 10^{-6} M vitamin B_{12} on V-MoS_2/Si, (e, f) 10^{-5} M vitamin B_{12} on V-MoS_2/ SiO_2-Si and (g, h) 10^{-4} M vitamin B_{12} on H-MoS_2/SiO_2-Si.*

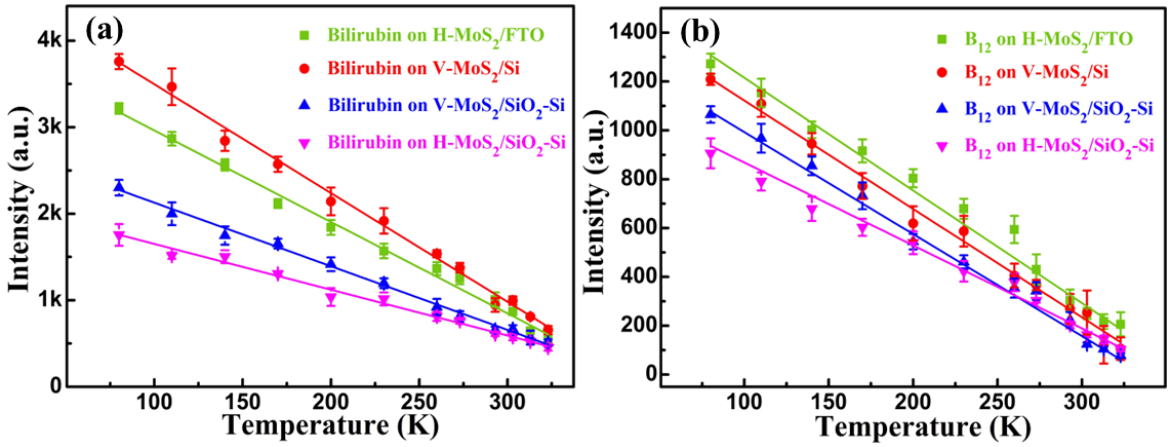

Figure 6.21 *Raman intensity versus temperature of (a) bilirubin and (b) vitamin B_{12} on H-MoS_2/FTO, V-MoS_2/Si, V-MoS_2/SiO_2-Si and H-MoS_2/SiO_2-Si.*

6.4 Conclusion

In conclusion, we have successfully synthesized large area semiconducting MoS_2 nanostructures with different morphologies on different substrates (FTO, Si and SiO_2-Si) via CVD method and used them as the SERS substrate for high level detection of bilirubin and vitamin B_{12}. The SERS detection limit of bilirubin on H-MoS_2/FTO, V-MoS_2/Si, V-MoS_2/SiO_2-Si and H-MoS_2/SiO_2-Si SERS substrates are found to be 10^{-11}, 10^{-11}, 10^{-9} and 10^{-8} M with EF values 4.9×10^7, 7.4×10^7, 1.7×10^6 and 1.7×10^5, respectively. The SERS detection limit of vitamin B_{12} on H-MoS_2/FTO, V-MoS_2/Si, V-MoS_2/SiO_2-Si and H-MoS_2/SiO_2-Si SERS substrates are found to be 10^{-8}, 10^{-8}, 10^{-7} and 10^{-6} M with EF values 8.1×10^4, 7.1×10^4, 9.2×10^3 and 1.2×10^3, respectively. The high SERS performance is due to coupling of PICT with the molecular resonance. The PICT process was verified by observing the decline of room temperature PL of biomolecules adsorbed SERS substrate. The SERS intensity can be enhanced by increasing the photo-induced electron density in the CB of the SERS substrate and this can be achieved at low temperature. At low temperature, the photo-induced electron density increases largely because of effectively decline of non-radiative recombination at low temperature. This will promote the charge transfer from SERS substrate to biomolecule under light illumination, proposing a useful approach for facilitating PICT

transitions and amplifying the Raman scattering cross-section. This has been understood by performing temperature-dependent SERS for both the biomolecules, showing the enhanced SERS signal at lower temperatures. Our results show that the high detection of biomolecules can be achieved with large area grown H-MoS_2/FTO and V-MoS_2/Si SERS substrates. Also, the new low temperature enhanced PICT process may find new insights for practical applications. Our study illuminates a new pathway for the use of MoS_2 as a SERS active material for biomolecule sensing.